

Cyclometalated Platinum(II) with Ethynyl-Linked Azobenzene Ligands: an Original Switching Mode

Paul Savel,^a Camille Latouche,^a Thierry Roisnel,^a Huriye Akdas-Kilig,^a Abdou Boucekkine,^{*a} Jean-Luc

Fillaut^{*a}

5 The photophysical properties of 6-phenyl-2,2'-bipyridyl platinum(II) complexes bearing different σ -alkynyl-linked azobenzene ancillary ligands were investigated. These complexes exhibit strong, broad, structureless charge-transfer bands in the visible region, which were red-shifted when the electron-donating ability of the para substituent on the azo-acetylide ligand increases. When excited at the charge-transfer absorption band, the complexes exhibit weak green emission, which is assigned to a triplet metal-to-ligand charge transfer/intraligand charge transfer emission ($^3\text{MLCT}/^3\text{L}^*\text{LCT}$). The presence of an amino substituent in the azobenzene moiety opened
10 the possibility of protonation which led to the formation of an azonium based derivative and resulted in drastic perturbations of the molecular orbitals and photophysical properties of the Pt-acetylide complex. These studies are fully supported by DFT and TD-DFT calculations.

Introduction

15 Among the cyclometalated square-planar platinum(II) complexes, 6-phenyl-2,2'-bipyridyl ($\text{C}^{\wedge}\text{N}^{\wedge}\text{N}$) platinum acetylide complexes attract a great deal of attention owing to their specific photophysical properties and potential applications in light-emitting devices,¹ conversion of solar energy,² nonlinear optical
20 devices,³⁻⁴ and chemosensors.⁵⁻⁸ These complexes exhibit charge-transfer absorption in the visible region and long-lived, relatively intense emission at room temperature in solution.¹⁻² In addition, their photophysical properties can be tuned by structural modification of the acetylide or 6-phenyl-2,2'-bipyridyl ligands to
25 meet the different requirements for assigned applications. For instance, Che and co-workers demonstrated the effect of para-substituents on aryl-acetylide ligands (L^*) on the photophysical properties of the Pt(II) $\text{C}^{\wedge}\text{N}^{\wedge}\text{N}$ complexes.¹ The metal-to-ligand charge transfer ($^1\text{MLCT}$) ($\text{L} = \text{C}^{\wedge}\text{N}^{\wedge}\text{N}$) absorption band energy
30 and the properties of the excited states are highly sensitive to the electron-donating or electron-withdrawing ability of the para substituent on the phenylacetylide ligand. We and others demonstrated that the para-position of the phenylacetylide group can be utilized for the luminescence sensing of ionic species.^{5, 7-11}
35 More recently, our group studied the importance of switching of reverse charge transfers in these species as a rational approach to luminescence sensing of ionic species (cations and anions).^{7-8, 10, 12} Such switches result in severe perturbations of the photophysical properties of the complexes which are reflected by
40 dramatic changes in wavelengths, lifetimes or quantum yields.

In the present work, we focus on the synthesis, characterization and photophysical studies of ($\text{C}^{\wedge}\text{N}^{\wedge}\text{N}$)Pt(II)-ethynyl-linked azobenzene complexes. Among several photochromic molecules,

azobenzene derivatives have been extensively investigated both
45 experimentally and theoretically, for their use as molecular devices i.e. individual molecule optomechanics,¹³⁻¹⁵ photocontrol of magnetic bistability,¹⁶ conductivity,¹⁷ macromolecular and supramolecular systems,¹⁸⁻²³ surface patterning,²⁴⁻²⁶ holographic information storage²⁷⁻²⁸ as well as photoregulation of
50 biomolecules.²⁹ Another interesting feature of the azobenzene derivatives is that their electronic transitions can be modulated by substituents attached to phenyl rings, allowing the tuning of their photophysical properties.³⁰ In the case of electron donor substituents, as amino groups, there is a substantial red shift
55 regarding the lower energy electronic transition in comparison to azobenzene molecule.³¹

Finally, the presence of amino substituents in the azobenzene moiety opens the possibility of protonation of distinct basic sites, whose equilibrium involves two tautomeric species, namely the
60 ammonium and the azonium tautomers.³²⁻³⁵ These transformations open an interesting possibility for the use of such systems in chemical sensors and switches that exploit binding-induced perturbation of the electronic structure of the extended π -conjugated system.

65 If the synthesis of transition metal complexes with azo substituents attracts current interest in order to associate the photoswitching properties of azobenzene with the electrochemical,³⁶ luminescent,³⁷ or magnetic,³⁸⁻³⁹ properties of metal complexes, less attention has been paid to the study of the
70 tautomeric (azonium-ammonium) equilibrium in transition metal based species. The goal of the current study was thus to investigate both experimentally and theoretically the photophysical properties of ($\text{C}^{\wedge}\text{N}^{\wedge}\text{N}$)Pt(II)-ethynyl-linked azobenzene complexes. In particular, we discuss the perturbation
75 of the electronic structure of the extended π -conjugation and

photophysical changes of a cyclometalated square-planar platinum(II) complex bearing a 4-N,N-dibutylamino-4'-ethynyl-azobenzene ligand, which revealed to be highly sensitive to acidic traces.

Experimental Section

Synthesis.

All manipulations were performed using Schlenk techniques under an Ar atmosphere. All commercially available starting materials were used as received. All solvents were dried and purified by standard procedures. The starting complex, [Pt(tBu₂-C[^]N[^]N)Cl], was prepared according to previously published methods. **1a,b** were obtained as previously described.⁴⁰⁻⁴¹

Physical Measurements and Instrumentation.

NMR spectra were recorded on AV 400 MHz or AV 500 MHz spectrometers.¹H and ¹³C chemical shifts are given versus SiMe₄ and were determined by reference to residual ¹H and ¹³C solvent signals. High resolution mass spectra (HRMS) were performed on a MS/MS ZABSpec TOF at the CRMPO (Centre de Mesures Physiques de l'Ouest) in Rennes. UV-vis absorption spectra were recorded using a UVIKON 9413 or Biotek Instruments XS spectrophotometer using quartz cuvettes of 1 cm path-length.

Luminescence spectra were measured in dilute degassed cyclohexane, dichloromethane, acetonitrile or Me-THF solutions ($\approx 10^{-6}$ M) using a FS920 steady-state fluorometer (Edinburgh Instruments). The spectra shown are corrected for the wavelength dependence of the detector, and the quoted emission maxima refer to the values after correction. Luminescence quantum yields were determined using the method of continuous dilution, using [Ru(bpy)₃]Cl₂ as the standard ($\Phi = 0.095$ in deaerated acetonitrile solution)⁴² and correcting for the refractive index.

Synthesis of 2a. [Pt(tBu₂-C[^]N[^]N)Cl] (100 mg, 0.174 mmol) was added to a suspension of alkyne **1a** (53 mg, 0.159 mmol), CuI (5.0 mg, 25 μ mol) and K₂CO₃ (200 mg) in 10 mL of deoxygenated methanol and methylene chloride (1:3 v/v). The mixture was stirred at room temperature overnight. After evaporation of the solvents, the crude residue was purified by column chromatography on silica gel with dichloromethane/methanol/triethylamine (98/2/0.5) as eluent to give **2a** as a red solid (274 mg, 63%). ¹H NMR (CD₂Cl₂, 400 MHz): δ 9.12 (d, $J = 5.6$ Hz, 1H), 7.94 (s, 1H), 7.91 (d, $J = 6.9$ Hz, 1H), 7.83 (d, $J = 8.7$ Hz, 2H), 7.77 (d, $J = 8.1$ Hz, 2H), 7.70 (s, 2H), 7.64 (d, $J = 5.6$ Hz, 1H), 7.59 (d, $J = 8.1$ Hz, 2H), 7.52 (d, $J = 6.9$ Hz, 1H), 7.20-7.10 (m, 4H), 6.74 (d, $J = 8.7$ Hz), 3.40 (m, 4H), 1.66 (m, 4H), 1.49 (s, 9H), 1.45 (s, 9H), 1.43 (m, 4H), 1.00 (t, $J = 7.3$ Hz, 6H). ¹³C NMR (CDCl₃, 125 MHz): δ 165.13, 163.42, 163.40, 158.10, 154.43, 151.58, 150.54, 150.18, 147.08, 143.38, 142.35, 138.58, 132.38, 131.24, 130.27, 124.93, 124.55, 124.09, 123.47, 121.98, 119.09, 115.45, 114.46, 111.12, 109.30, 107.03, 50.96, 35.97, 35.69, 30.57, 30.35, 29.53, 20.34, 14.00. Anal. found: C, 62.59; H, 6.13; N, 7.73. C₄₆H₅₃N₅Pt \cdot 1/2H₂O Calc.: C, 62.78; H, 6.148; N, 7.96. m/z (Zabspec-TOF) 909.3585, 893.3843, 871.4009; ([M+K]⁺, C₄₆H₅₃N₅¹⁹⁵PtK requires 909.3585 (0 ppm); [M+Na]⁺, C₄₆H₅₃N₅¹⁹⁵PtNa requires 893.3846 (0 ppm); [M+H]⁺, C₄₆H₅₄N₅¹⁹⁵Pt requires 871.4027 (2 ppm)).

Synthesis of 2b. The same procedure applied to [Pt(tBu₂-C[^]N[^]N)Cl] (118 mg, 0.206 mmol), **1b** (50 mg, 0.216 mmol), CuI

(5.0 mg, 25 μ mol) and K₂CO₃ (220 mg, 1.45 mmol) in 10 mL of deoxygenated methanol and methylene chloride (1:3 v/v) gave **2b** as a red solid (181 mg, 47%). ¹H NMR (CD₂Cl₂, 400 MHz): δ 9.01 (d, $J = 5.7$ Hz, 1H), 8.02 (d, $J = 8.2$ Hz, 2H), 7.94 (d, $J = 8.3$ Hz, 2H), 7.89 (s, 1H), 7.84 (d, $J = 8.3$ Hz, 2H), 7.78 (d, $J = 7.2$ Hz, 1H), 7.66-7.56 (m, 4H), 7.56 (dd, $J = 5.4$; 1.2 Hz, 1H), 7.44 (d, $J = 7.2$ Hz, 1H), 7.13 (m, 2H), 1.48 (s, 9H), 1.46 (s, 9H). ¹³C NMR (CDCl₃, 125 MHz): δ 165.16, 163.80, 163.69, 158.10, 155.02, 154.40, 151.54, 149.60, 147.11, 142.05, 138.50, 134.00, 133.17, 132.58, 131.34, 124.62, 124.22, 123.71, 123.41, 123.16, 119.20, 118.74, 115.57, 114.53, 114.27, 112.14, 107.21, 36.02, 35.74, 30.56, 30.35. Anal. found: C, 60.97; H, 5.51; N, 7.77. C₃₉H₃₅N₅Pt Calc.: C, 60.93; H, 4.59; N, 9.11. m/z (Zabspec-TOF), 807.2169, 791.2429, 769.2611; ([M+H]⁺, C₄₆H₅₃N₅¹⁹⁵PtK requires 807.21719 (0 ppm); [M+Na]⁺, C₄₆H₅₃N₅¹⁹⁵PtNa requires 791.24325 (0 ppm); [M+H]⁺, C₃₉H₃₆N₅¹⁹⁵Pt requires 769.26131 (0 ppm)).

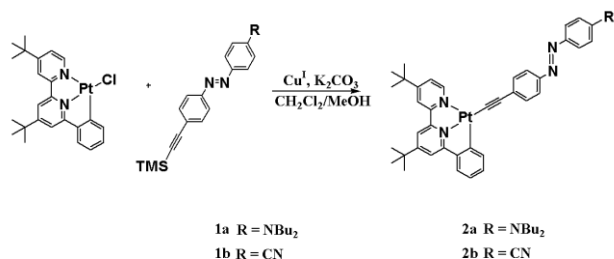
Crystallographic Structure Determinations. (C₄₁H₃₇Cl₆N₅Pt); $M = 1007.55$. APEXII, Bruker-AXS diffractometer, Mo-K α radiation ($\lambda = 0.71073$ Å), $T = 150(2)$ K; monoclinic $P 2_1/c$ (I.T.#14), $a = 11.8455(3)$, $b = 23.7605(6)$, $c = 15.3741(4)$ Å, $\beta = 107.0200(10)^\circ$, $V = 4137.60(18)$ Å³. $Z = 4$, $d = 1.617$ g.cm⁻³, $\mu = 3.815$ mm⁻¹. The structure was solved by direct methods using the SIR97 program,⁴³ and then refined with full-matrix least-square methods based on F^2 (SHELXL-97)⁴⁴ with the aid of the WINGX program.⁴⁵ All non-hydrogen atoms were refined with anisotropic atomic displacement parameters. H atoms were finally included in their calculated positions. A final refinement on F^2 with 9441 unique intensities and 484 parameters converged at $\omega R(F^2) = 0.1327$ ($R(F) = 0.0497$) for 6939 observed reflections with $I > 2\sigma(I)$.

Computational studies. Density functional theory (DFT) calculations were performed using the standard B3LYP functional⁴⁶⁻⁴⁸ and a double zeta LANL2DZ basis set,⁴⁹ augmented with polarization functions on all atoms except hydrogen ones (exponents equal to 0.587 and 0.736 respectively for the d functions of C and N, and 0.8018 for the f function of Pt) with the Gaussian09⁵⁰ program. The geometries of complexes **2a**, **2b** and **2a-H⁺** in their singlet ground-state have been optimized and all stationary points were fully characterized as true minima on the potential energy hypersurface via analytical vibrational frequency calculations. Solvent (CH₂Cl₂) effects have been taken into account using the PCM model.⁵¹⁻⁵² The computations of the electronic absorption spectra using time-dependent DFT (TD-DFT) were carried out at the same level. In order to estimate the phosphorescence wavelengths, the relaxed triplet states geometries of the complexes have been obtained using both TD-DFT and unrestricted DFT computations. Drawings of molecular structures and orbitals were done using the Molekel program⁵³ whilst theoretical absorption spectra were plotted using Swizard,⁵⁴ the half-bandwidths for the Gaussian model being taken equal to 2000 cm⁻¹. Percentages compositions of molecular orbitals (MOs) were computed using the AOMix program.⁵⁵

Results and Discussion

The synthesis of the azo containing [Pt(tBu₂-C[^]N[^]N)(C \equiv C-C₆H₄-N=N-C₆H₄-R)] (tBu₂-C[^]N[^]N = 4,4'-di(tert-butyl)-6-phenyl-2,2'-

bipyridine; R = NBu₂ (**2a**), R = CN (**2b**) was obtained by reaction of the [Pt(tBu₂-C[^]N[^]N)Cl]¹ precursor with the substituted azo-alkynes **1a,b**^{1, 40-41} in the presence of a catalytic amount of CuI and K₂CO₃. The complexes were characterized by ¹H and ¹³C NMR, HRMS, and elemental analysis.



Scheme 1. Synthetic route to **2a,b**. K₂CO₃, CuI, CH₂Cl₂/MeOH, 16h, r.t. (**2a**: 63 %; **2b**: 47 %).

Crystal Structure Determination. Suitable crystals of **2b** were obtained in a few days upon slow diffusion at room temperature of pentane into a CH₂Cl₂ solution of the complex. An ORTEP diagram of complex **2b** is shown in Figure 1. The unit cell, data collection, and refinement parameters are summarized in Table S1 (ESI) with selected bond lengths and angles for both structures given in Table 1. The complex exhibits a distorted square planar coordination geometries around the Pt(II) nucleus. The Pt-N distance to the central pyridine, the Pt-C(aryl) and the Pt-C(acetylide) distances, 1.986(5), 1.990(7) and 1.974(7) Å, respectively, are slightly shorter than the peripheral Pt-N distance of 2.110(6) Å. These values are in the expected range of 2.0 Å and are thus consistent with earlier reports of similar structures.^{1, 7} The azobenzene moiety is not coplanar with the phenylacetylide fragment (dihedral angle C(21)–Pt(1)–C(33)–C(34) 25.49°). Neither π–π nor intermolecular Pt···Pt contacts were observed; the nearest Pt···Pt distance is 6.757 Å.

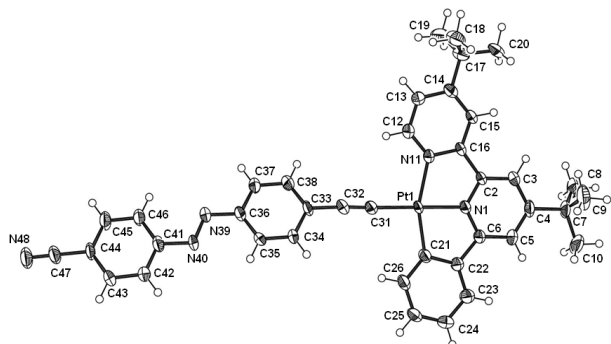


Figure 1. An ORTEP plot for **2b** drawn with thermal ellipsoids at the 50% probability level. T = 150 K.

Table 1. Selected Bond Lengths (Å) and Angles (deg) for Complex **2b**

Pt(1)-N(1) 1.986(5)	Pt(1)-C(21) 1.990(7)
C(31)-C(32) 1.184(10)	Pt(1)-N(11) 2.110(6)
Pt(1)-C(31) 1.974(7)	
C(31)-Pt(1)-N(1) 178.7(3)	C(31)-Pt(1)-C(21) 97.7(3)
N(1)-Pt(1)-C(21) 81.8(2)	C(31)-Pt(1)-N(11) 102.3(2)
N(1)-Pt(1)-N(11) 78.2(2)	

Photophysical properties. The UV–vis absorption spectra of **2a,b** in dichloromethane solution are presented in Figure 2, and the band maxima and molar extinction coefficients for each complex are compiled in Table 2. The absorption obeys Lambert–Beer’s law in the concentration range studied (1 × 10^{−6} through 1 × 10^{−4} mol/L), suggesting no aggregation of the complexes within this concentration range. In line with the previous work on cyclometalated platinum(II) complexes, the intense absorption bands around 250–350 nm are assigned to the intraligand (IL) π,π* transitions.¹ The broad, intense absorption bands at 400–550 nm are assigned to mixed ¹MLCT (metal-to-ligand charge transfer)/¹L’LCT (ligand-to-ligand charge transfer)/¹ILCT (intraligand charge transfer) transitions considering the energy and intensity of these bands, compared to those reported in the literature for other platinum C[^]N[^]N acetylide complexes.^{3, 7-9, 56} The low-energy absorption bands of the complexes appear to show two distinct transitions (**2a**: 470 and 432 nm; **2b**: 450 and 425 nm). The transitions appearing at lower energies are influenced significantly by the nature of the *para* substituent on the phenylacetylide ligand L’. The electron-withdrawing substituent CN induces a blue-shift compared to complex **2a** (**2a**: 470 nm; **2b**: 450 nm). The involvement of n,π* and π,π* transitions of this azo containing ligand into these low-energy absorption bands should also be taken into account considering the energy and intensity of such bands in **1a,b** and similar azobenzene derivatives.⁵⁷

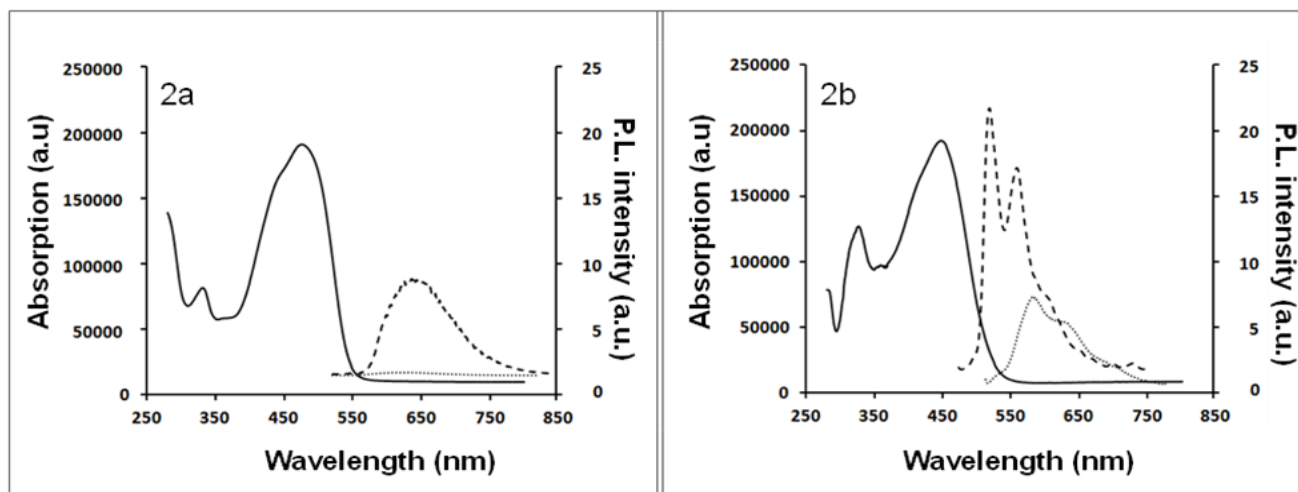


Figure 2. UV-vis absorption spectra of Pt(II) complexes **2a,b** in dichloromethane solution (2.0×10^{-5} M, 293 K) (—). RT (Cyclohexane) (···) and frozen emission spectra (Me-THF) (---) of complexes **2a,b** (5×10^{-6} mol/L). The excitation wavelength was 450 nm for **2a** and **2b**.

Table 2. Photophysical Parameters of **2a,b**, **2a-H⁺**

	$\lambda_{\text{abs}}^{\text{a}}/\text{nm}$ ($\epsilon/10^3 \text{ L} \cdot \text{mol}^{-1} \cdot \text{cm}^{-1}$)	$\lambda_{\text{em}}^{\text{a}}/\text{nm}$	$\lambda_{\text{em}}^{\text{b}}/\text{nm}$	$\lambda_{\text{em}}^{\text{c}}/\text{nm}$
2a	280 (33.0), 332 (18.0), 432 (40.0), 470 (45.0)	595	600	625
2a-H⁺d	280 (32.0), 350 (18.0), 570 (25.0)	580, 630	-	575, 635
2b	280 (28.0), 330 (15.2), 425 (18.0), 450 (22.1)	585	580, 635, 690	520, 570, 620

a. Measured at room temperature, in dichloromethane; b. Measured at room temperature, in cyclohexane c. Measured at 77 K in Me-THF, 5×10^{-6} mol/L ($\lambda_{\text{exc}} = 450$ nm); d. upon addition of 1.5 eq. of $\text{CF}_3\text{CO}_2\text{H}$, in dichloromethane or Me-THF.

Although the transitions occurring in the region of 420–440 nm are less sensitive to the effects of *para* substituents on the azo-acetylide ligand, a similar trend was observed for these transitions (**2a**: 432 nm; **2b**: 425 nm), which likely originate from the $d\pi$ (Pt) $\rightarrow \pi^*(\text{C}^{\wedge}\text{N}^{\wedge}\text{N})$ MLCT. A similar effect of the *para* substituent at the phenylacetylide ligand on the charge-transfer band energy has been reported by Che's group for $[\text{Pt}(\text{tBu}_2\text{C}^{\wedge}\text{N}^{\wedge}\text{N}) (\text{C}\equiv\text{C}-\text{C}_6\text{H}_4-\text{R})]$ complexes without the 4-phenyl substituent.¹ The more electron rich acetylide ligand with the electron-donating dibutylamino-substituent raises the Pt *d* orbital energy, which leads to a decrease of the energy gap between the bipyridine-based LUMO and the Pt-based HOMO and results in the observed red-shift, compared to **2b**.

Continuous irradiation of **2a,b** in hexane with 450 nm radiation did not result in a *trans* \rightarrow *cis* isomerization. This observation indicates that the irradiation generates excited states that decay without isomerization. This is in line with the above discussion and the assumption of a bipyridine-based character of the lowest unoccupied MOs of complexes **2a,b**.

The emission characteristics of complexes **2a,b** in cyclohexane, dichloromethane and acetonitrile at room temperature were first investigated. Excitation of the complexes in cyclohexane solution at their respective charge-transfer band at room temperature results in very weak luminescence. **2a** is almost non emissive (Figure 2a) even at low temperature. Even if also weakly emissive at room temperature, **2b** shows an almost structured emission profile (Figure 2b). Its frozen solution emission spectrum appears at a shorter wavelength, as frequently observed

in related complexes.^{1, 8, 58} This frozen solution emission has a well structured emission profile that spans the range of ca. 500–700 nm (with vibrational progressions of around 1350 cm^{-1} , typical of the ring-breathing mode of the 6-phenyl-2,2'-bipyridyl ligand).^{1, 8, 58} Conversely, the spectrum observed from frozen solutions of **2a** (Me-THF) does not exhibit vibronic structure and this complex emits at a longer wavelength, compared to **2b**. The values of the Stokes shift (**2b**, almost 5800 cm^{-1} at r.t.) suggest that the observed emission from these complexes is from a triplet excited state. With reference to the other platinum ($\text{tBu}_2\text{C}^{\wedge}\text{N}^{\wedge}\text{N}$) complexes reported in the literature, the emission could be tentatively assigned to the $^3\text{MLCT}/^3\text{L}'\text{LCT}$ emission.^{1, 10, 59} The charge transfer nature of the emitting state is also supported by the vibronic feature of the emission spectra at low temperature. Finally, the solvents also influence the emission quantum yield pronouncedly: as commonly observed in Pt(II) complexes with a $^3\text{MLCT}$ emitting state, **2b** is more emissive in less polar solvents : [$\phi_{\text{DCM}} = 1.8 \times 10^{-3}$; $\phi_{\text{MeCN}} = 0.2 \times 10^{-3}$]. The emission intensity for **2a** is much lower [$\phi_{\text{DCM}} = 0.2 \times 10^{-3}$]. This is in line with general observations for ($\text{tBu}_2\text{C}^{\wedge}\text{N}^{\wedge}\text{N}$) platinum acetylide complexes with a strong electron-donating substituent on the phenylacetylide ligand, for which the lifetimes are much shorter and the emission quantum yields are much lower.¹ This could be attributed to the presence of a low-lying $^3\text{L}'\text{LCT}$ state, which adds an additional decay pathway. At the opposite, substituents with large electron-withdrawing abilities raise the $\text{L}'\text{LCT}$ excited-state energy, thus lowering its contribution to the emissive state.

Computational results (ground state). The optimized structural parameters of **2b** in the S0 ground state are in good agreement with the X-ray structural analysis data. The computed optimized bond lengths of complex **2b** are in the range of the observed ones for the Pt-C bonds (2.001 Å vs. [1.990] Å for Pt(1)-C(21) and 1.950 Å vs. [1.974] Å for Pt(1)-C(31)) or slightly longer for Pt-N ones (2.018 Å vs. [1.986] Å for Pt(1)-N(1) and 2.183 Å vs. [2.110] Å for Pt(1)-N(11)). In particular, the computed C(31)-C(32) bond length (1.243 Å) appears slightly larger than the observed one (1.184 Å). This phenomenon has already been described for similar inorganic complexes.^{10, 60} The computed dihedral angle (C(21)-Pt(1)-C(33)-C(34)) equal to 73.08° (25.49° observed) confirms that the azobenzene and phenylacetylide moieties are not coplanar. This difference between the computed and X-ray dihedral angle can be due to packing effects; indeed the rotation barrier between the computed and X-ray conformations is very weak (< 0.4 kcal.mol⁻¹). The computed bond lengths and the (C(21)-Pt(1)-C(33)-C(34)) dihedral angle of complex **2a** are similar to those of complex **2b**.

The molecular orbital diagram of both complexes is depicted on Figure 4. As expected, HOMO of **2a** exhibits an important contribution of the NBU₂ group. The HOMO -1 and the HOMO -3 are almost totally localized on the Pt-C≡C moiety of the molecule. The HOMO-4 orbital is mainly localized on the phenyl group of the L ligand. The LUMO of complex **2a** is localized on the bipyridine ligand whereas the LUMO +1 is mainly localized on the diazo moiety; the same localization appears for LUMO +2 (not depicted on Figure 4 for clarity).

Similarly, most of the HOMOs of compound **2b** are also localized on Pt and on the L' ligand. However, the LUMO of this complex is not localized on the L moiety but on the diazo part of the L' one and partly on the nitrile withdrawing group. This difference is explained by the strong accepting character of CN in para of the azobenzene.

TD-DFT calculations were performed on both complexes. The computed absorption wavelengths (λ) and oscillator strengths (f) are reported in Table 3 and the simulated spectra of **2a** and **2b** are depicted on Figure 3. A perfect agreement can be observed between the computed (293 nm and 341 nm) and experimental (280 nm and 332 nm) values for the highest energy bands of complex **2a** (respectively 284 nm and 341 nm vs. 280 nm and 330 nm for complex **2b**). The computed absorption bands at 433 nm (HOMO → LUMO +2 (80 %)) for complex **2a** and 413 nm (HOMO -3 → LUMO (58 %) + HOMO -2 → LUMO +1 (38 %)) for complex **2b** are in good agreement with experimental values, at 432 nm (**2a**) and 425 nm (**2b**). These bands can be assigned to a mix of MLCT and L'LCT for both complexes and to a IL'CT excitation, in the case of complex **2a**.

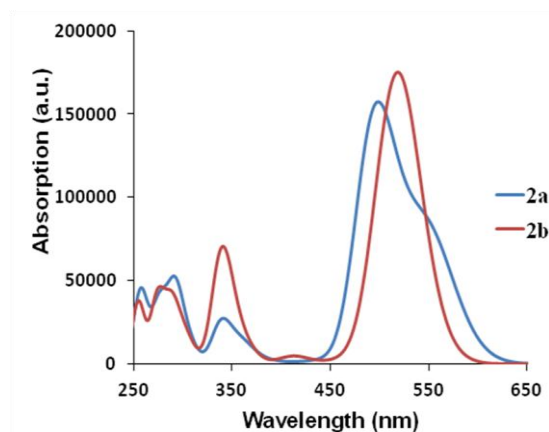
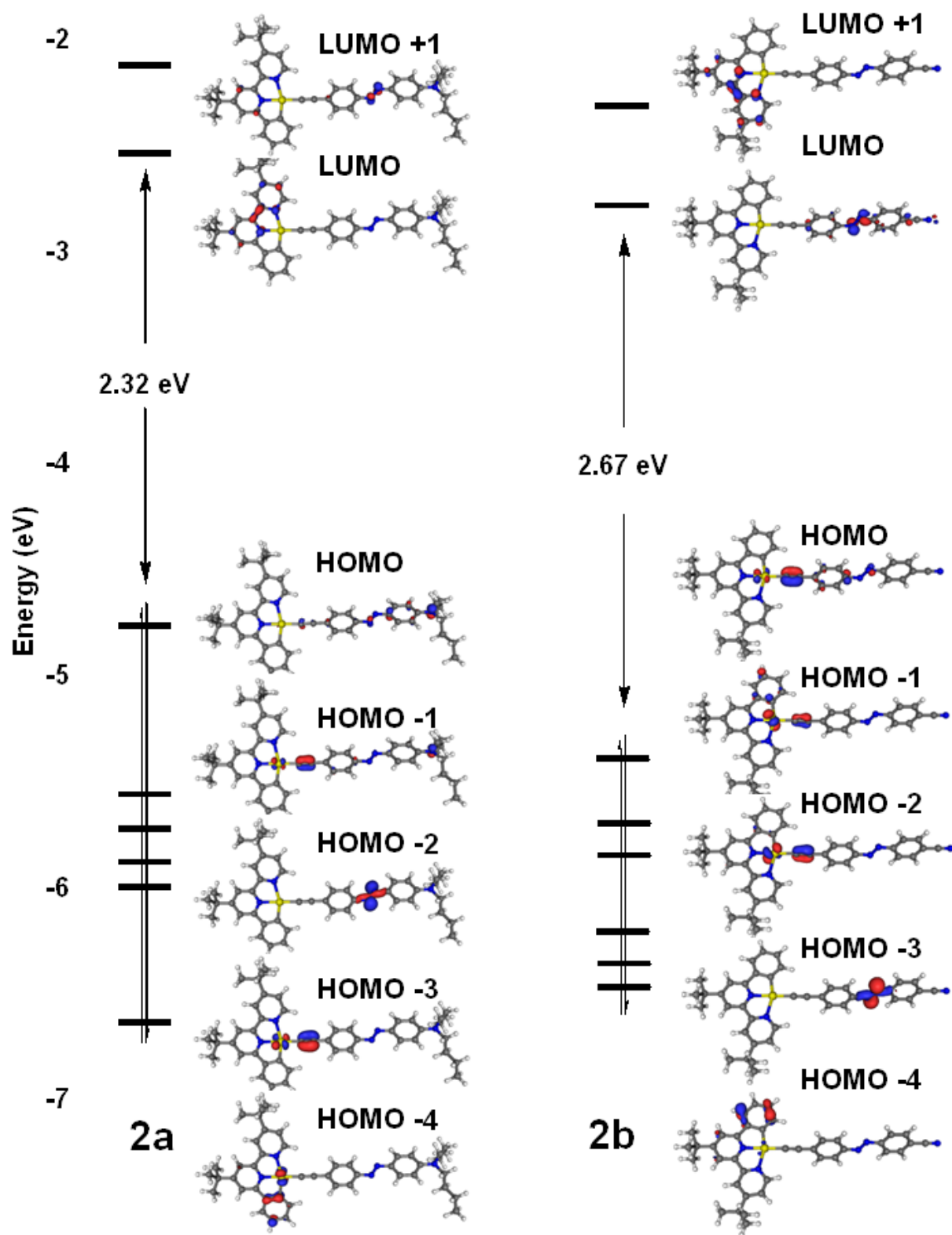


Figure 3. Simulated UV-Visible spectra of **2a** and **2b**.

The lowest energy absorption band experimentally observed at 470 nm for **2a** can be related to calculated excitations at 500 nm (HOMO to LUMO) and 533 nm (HOMO to LUMO +1), which correspond to charge transfers from the L' moiety to both L' and L moieties (IL'CT and L'LCT).

Similarly, the lowest energy absorption band experimentally observed for **2b** can be attributed to a mix of HOMO and HOMO -2 to LUMO transitions. The experimental red shift of the lowest energy absorption band between complexes **2a** and **2b** (20 nm experimentally) is also well reproduced by the TD-DFT calculations (35 nm), as expected on the basis of the respective HOMO-LUMO gaps.

The phosphorescence wavelengths of **2a** and **2b** have been computed using TD-DFT, carrying out geometry optimizations of the first triplet states of the molecules. In the case of **2b**, two low energy triplet states have been found, respectively at 620 and 580 nm above the singlet ground state, values which are in agreement with the experimental observation. An in-depth investigation of these two triplets showed that their relaxed geometries differ, more particularly by the C(21)-Pt(1)-C(33)-C(34) dihedral angle (see Figure 1) respectively equal to 43° and -3° for the first (at 620 nm) and second (at 580 nm) triplet states, so that the first one exhibits a more planar conformation than the second. We remind that the computed dihedral angle in question is equal to 73.08° for **2b** in the ground state (X-ray value, 25.49°). The planarity of the complex is a key factor driving its electronic structure and optical properties. As a consequence, the two different geometries lead to different frontier MOs (MO diagrams and composition of the MOs involved in the transitions are given in figure S1 and table S3 of the SI). Moreover, the nature of the two triplet states is different (see figure S1 of the SI); the second one is a ³ML'CT/³LL'CT excited state while the first one is mainly a ³MLCT expected to be more emissive. In the case of **2a**, the TD-DFT computations led us to find a first triplet state at 697 nm above the ground state; this value slightly overestimates the wavelength of the weak emission observed from 600 to 700 nm.



5 **Figure 4.** Frontier MO diagrams of **2a** and **2b**.

Table 3. TD-DFT computed spectra of **2a** and **2b** [experimental wavelengths are reported between square brackets].

Complex	λ_{calc} nm ; (f ^a)	λ_{max} [exp], nm	Transitions (% weights)
2a	550 (0.69)	553 [470]	HOMO → LUMO (93 %)
	497 (1.39)		HOMO → LUMO +1 (95 %)
	438 (0.01)	433 [432]	HOMO → LUMO +2 (80 %)
	357 (0.07)	341 [332]	HOMO → LUMO +3 (37 %)
	339 (0.22)		HOMO -3 → LUMO +2 (36 %)
	295 (0.16)	293 [280]	HOMO -6 → LUMO (80 %)
	292 (0.18)		HOMO → LUMO +4 (47 %)
			HOMO -8 → LUMO (21 %)
			HOMO -6 → LUMO +2 (66 %)
2b	519 (1.59)	518 [450]	HOMO → LUMO (95 %)
	491 (0.04)		HOMO -2 → LUMO (88 %)
	414 (0.04)	413 [425]	HOMO -3 → LUMO (58 %)
	352 (0.13)		HOMO -2 → LUMO +1 (38 %)
	342 (0.22)	341 [330]	HOMO -2 → LUMO +2 (82 %)
	340 (0.13)		HOMO -6 → LUMO (75 %)
	337 (0.24)		HOMO -7 → LUMO (75 %)
	292 (0.20)	284 [280]	HOMO -4 → LUMO +1 (89 %)
	285 (0.12)		HOMO -4 → LUMO +2 (70 %)
			HOMO -11 → LUMO (43 %)
			HOMO → LUMO +5 (31 %)

Protonation studies. The presence of an amino substituent in **2a** prompted us to study the possibility of protonation of this compound in dichloromethane. When a dichloromethane solution of **2a** was treated by an acid (HCl, CF₃CO₂H), the solution immediately assumed a deep blue color. The UV-vis spectra of **2a** dissolved in neat methylene chloride and upon addition of a saturated HCl/diethylether are shown in Figure 5, making obvious the substantial shift of the lowest energy transition after addition of the HCl solution.

The intense band from 380 to 550 nm strongly decreases monotonically throughout the sequential addition of the saturated HCl/diethylether solution while a new band centred at ca. 555 nm concomitantly grows in. A well-defined isosbestic point at 502 nm is observed, suggestive of a ground-state equilibrium of two species. Addition of drops of triethylamine results in the recovery of the initial absorption spectrum, indicating the reversible nature of the protonation of **2a**. Let us notice that the addition of a saturated HCl/diethylether solution to **2b** in dichloromethane in similar conditions didn't result in any change. The addition of a stronger acid (trifluoroacetic acid) leads to the rapid degradation of this product.

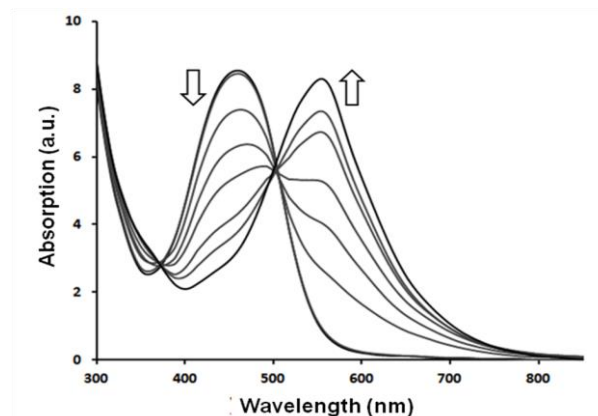


Figure 5. UV-Vis absorption spectral changes of **2a** (10^{-6} M) in CH₂Cl₂ upon addition of a saturated HCl/diethylether solution.

As in the majority of aminoazobenzenes, the protonated molecule **2a-H⁺** can be subject to ammonium–azonium tautomerism.³²⁻³⁵ Most azonium ions absorb above 500 nm. The band at ca. 555 nm was thus tentatively assigned to the azonium form of **2a-H⁺** as the predominant form.

The protonated **2a-H⁺** is non-emissive at room temperature (Figure 6). Meanwhile, at low temperature, **2a-H⁺** in dichloromethane solution produced luminescence at 580 and 630 nm, upon excitation at 500 nm, with vibrational progressions of around 1250 cm⁻¹. The apparent Stokes shift strongly decreases from **2a** to **2a-H⁺**. Considering that the azonium is a great deal more electron-withdrawing than the azobenzene substituent, we assume that an IL' excited state derived from the azonium moiety becomes lower lying in energy in comparison to the MLCT/L'LCT state in the neutral form. The emission is thus tentatively assigned as derived from an azonium based ¹IL' origin, as the predominant emissive state of the protonated form **2a-H⁺**.

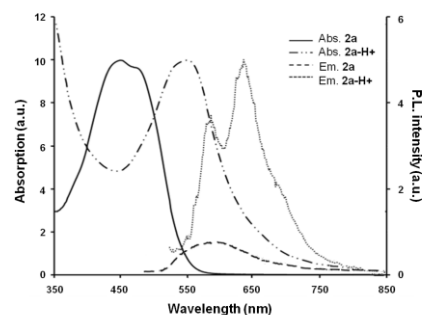
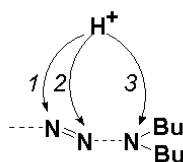
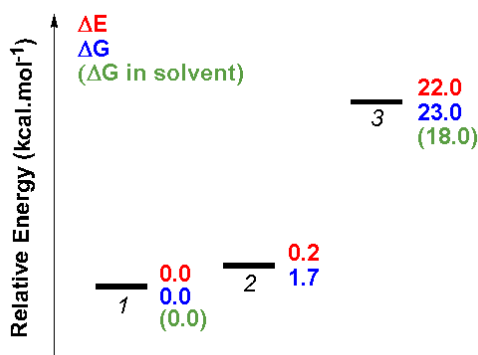


Figure 6. Normalized absorption of **2a** and **2a-H⁺** in CH₂Cl₂ and emission spectra at 77K in Me-THF. The excitation wavelength was 450 nm for **2a** and 500 nm for **2a-H⁺**.

Computational studies (2a-H⁺). In order to determine the structure of complex **2a-H⁺**, we considered the three possible protonation sites depicted in scheme 2. The geometries of the possible isomers were first optimized. Their normal modes of vibration were then determined. All optimized structures were checked to be true minima on the potential energy surface. Their electronic relative energies and their Gibbs free energies were computed (Scheme 3). In a first step, the calculations have been done in vacuum. Isomer 1 was found to be the most stable but its energy is very close to that of the isomer 2 (0.2 kcal.mol⁻¹ in energy, 1.7 kcal.mol⁻¹ in free Gibbs energy). Finally, the third protonation site, i.e. on the NBu₂ group, appears as the less suitable: the total energy of the isomer 3 is higher than that of the isomer 1 by ca. 22.0 kcal.mol⁻¹ (23.0 kcal.mol⁻¹ for Gibbs free energy).



Scheme 2. The three possible protonation sites of **2a**. 1 corresponds to the protonation at N(39); 2: N(40); 3: N(48).



Scheme 3. Relative energies (red) and Gibbs free energies (blue) of protonated isomers 1, 2 and 3 (vacuum). Between brackets, the computed values in solvent.

The second step of this computational study concerned the influence of the solvent (dichloromethane) on the relative stability of the different protonated isomers. First, carrying out geometry optimizations using the PCM model, it was found that isomer 1 is definitely more stable than isomer 3, by 16.2 kcal.mol⁻¹ (18.0 kcal.mol⁻¹ for Gibbs free energy). Interestingly, the same optimization process applied to isomer 2, did not permit to obtain a converged protonated structure. Thus, we used other functionals, among them M06, M06-2X, and larger basis sets, but in all cases it was not possible to get a correct convergence for the geometry of the protonated structure. This suggests that this site is not suitable for the protonation, in solution. These results confirm that the nitrogen atom N(39) (see figure 1) is the favoured protonation site thus leading to an azonium. In the following, we will only discuss the case of the isomer 1.

Structurally, the main differences between compound **2a** and **2a-H⁺** appear on the C(36)-N(39) and N(40)-C(41) bonds whose lengths become shorter after protonation (1.413 Å and 1.399 Å for the neutral species **2a** vs. 1.398 Å and 1.363 Å for the **2a-H⁺**) whereas the N=N distance becomes slightly longer (1.280 Å vs 1.296 Å, for complexes **2a** and **2a-H⁺** respectively).

The HOMO and LUMOs of complexes **2a** and **2a-H⁺** are dramatically different (Figure 7). First at all, the HOMO of **2a**, mainly localized on the NBu₂ unit disappears. The HOMO of the complex **2a-H⁺** is now mainly localized on the Pt-acetylide moiety with a participation of the NBu₂ unit, and is similar to the HOMO-1 of **2a**. The energy remains almost unchanged from the HOMO-1 of **2a** to the HOMO of **2a-H⁺**. At the same time, we can notice an important stabilization of the LUMO +1 of complex **2a**, localized on the di-azo moiety, which becomes the LUMO of **2a-H⁺**. This strong decrease of the energy leads to a smaller HOMO-LUMO gap (1.99 vs. 2.32 eV, respectively for complexes **2a-H⁺** and **2a**). Conversely, the LUMO of complex **2a** becomes the LUMO +1 for the complex **2a-H⁺** which keeps approximately the same energy as for the neutral species.

TD-DFT calculations for compound **2a-H⁺** (Figure 8 and Table 4) well reproduce the experimental shift of 100 nm observed for the lowest energy absorption bands (experimental values: 470 nm (**2a**) vs. 570 nm; computed values: 500-553 nm (**2a**) vs 625 nm (**2a-H⁺**)). The absorption band at 570 nm can be assigned to a mix of transitions from the HOMO to the LUMO, but also from HOMO -3 and the HOMO-4 to the LUMO. It can be described as resulting from ML'CT with some IL'CT and LL'CT participation (Table 4). The emission spectrum of **2a-H⁺** was then computed using TD-DFT calculations at the same level of theory, carrying out the geometry optimization of its first singlet excited state in CH₂Cl₂ solution.

Table 4. TD-DFT computed spectra of **2a-H⁺** [experimental wavelengths between square brackets].

Complex	λ_{calc} , nm ; (f [*])	λ_{max} [exp], nm	Transitions (% weights)
2a-H⁺	626 (1.74)	625	HOMO → LUMO (99 %)
	420 (0.37)	420 [570]	HOMO -4 → LUMO (70 %)
			HOMO-3 → LUMO (19 %)
	365 (0.09)	338 [350]	HOMO-1 → LUMO+2 (83%)
	337 (0.22)		HOMO-5 → LUMO +1 (82%)
	304 (0.13)		HOMO-1 → LUMO +3 (83 %)
	302 (0.22)		HOMO → LUMO +4 (72 %)
	291 (0.21)	298 [280]	HOMO-5 → LUMO +2 (79%)
	275 (0.14)	276	HOMO-8 → LUMO+1 (83 %)
	273 (0.15)		HOMO-9 → LUMO+1 (61 %)

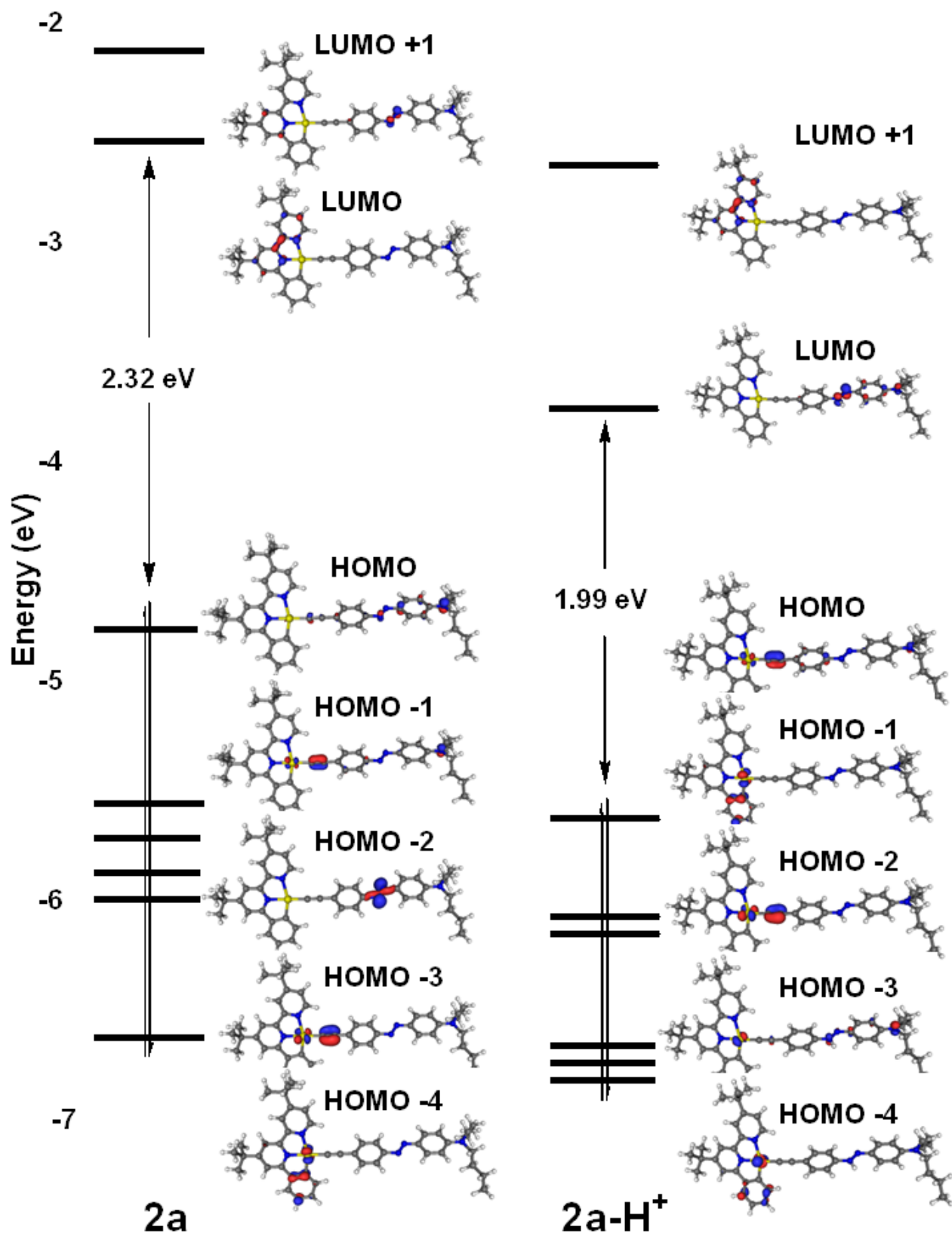


Figure 7. Frontier MO diagrams of **2a** and **2a-H⁺**

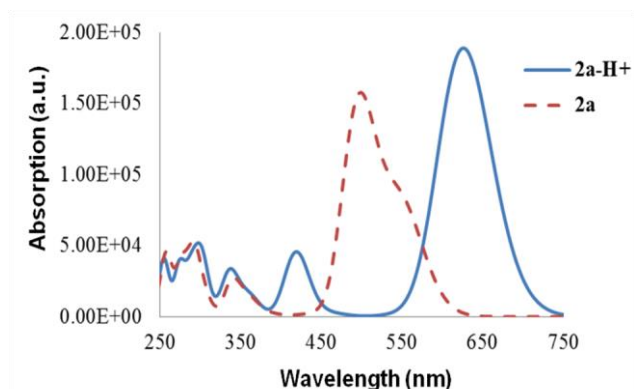


Figure 8. Simulated UV-Visible spectra of **2a** and **2a-H⁺**.

The computed fluorescence wavelength (690 nm), corresponding to a mix of ¹LL'CT and ¹IL'CT states, is in a reasonable agreement with the experimental value at low temperature (630 nm). Moreover, it is worth noting that the computed Stokes shift for **2a-H⁺** and the observed one are the same, *i.e.* 65 nm. Altogether, this DFT analysis supports well the hypothesis that the azonium tautomer *I* is the predominant species present in the acidic solution. Interestingly, this specific behavior leads to dramatic changes of both the HOMO and LUMO levels of the overall system. In this way, it dramatically differs from that of platinum acetylide complexes bearing amino moieties on the phenylacetylide unit for which the protonation of the amino substituent dramatically lowers the phenylacetylide-based molecular orbital and moves the Pt-based orbital as the HOMO.⁶¹⁻⁶²

Conclusions

The photophysics of two mononuclear cyclometalated platinum(II) 4,6-diphenyl-2,2'-bipyridyl acetylide complexes **2a,b** was investigated. Lowest energy absorption bands correspond to the superimposed absorptions of the (C[^]N[^]N) platinum acetylide fragment and that of the azobenzene entity. These broad, moderately intense ¹MLCT/¹ILCT/¹L'CT absorption bands at 400–550 nm are shifted in accordance with the electron-donating ability of the *para* substituent on the azo-containing phenylacetylide ligand. Excitation of these complexes in solution at their respective charge-transfer band results in weak luminescence that can be assigned to a ³MLCT/³LLCT emission, to which the azo unit does not interfere. Upon protonation, the azo-amino containing complex **2a** shows a substantial shift of the lowest energy transition, which is related to the formation of a preponderant azonium species **2a-H⁺**, whose emission was tentatively assigned to a ¹IL' origin. The photophysical properties of the (C[^]N[^]N) platinum acetylide fragment were then masked. DFT and TD-DFT calculations allowed us to accurately describe the perturbations of both HOMO and LUMOs orbitals of **2a** upon its protonation, allowing the observed properties to be rationalized.

Aknowledgements

The authors are grateful to GENCI-IDRIS and GENCI-CINES for an allocation of computing time (Grant No. 2012-080649).

Notes and references

- ^a Institut des Sciences Chimiques de Rennes UMR 6226 CNRS-Université de Rennes 1, 35042, Rennes Cedex France
E-mail: jean-luc.fillaut@univ-rennes1.fr; abdou.boucekkine@univ-rennes1.fr
- †Electronic Supplementary Information (ESI) available: [optimized geometries and computed excitation energies; CCDC 949194 contains the supplementary crystallographic data for complex **2b**. These data can be obtained free of charge from the Cambridge Crystallographic Database Center, 12 Union Road, Cambridge CB2 1EZ, UK (fax: +44 1223 336033; e-mail: deposit@ccdc.cam.ac.uk).]. See DOI: 10.1039/b000000x/
- W. Lu, B.-X. Mi, M. C. W. Chan, Z. Hui, C.-M. Che, N. Zhu and S.-T. Lee, *J. Am. Chem. Soc.*, 2004, **126**, 4958-4971.
- J. Schneider, P. Du, P. Jarosz, T. Lazarides, X. Wang, W. W. Brennessel and R. Eisenberg, *Inorg. Chem.*, 2009, **48**, 4306-4316.
- R. Liu, Y. Li, Y. Li, H. Zhu and W. Sun, *J. Phys. Chem. A*, 2010, **114**, 12639-12645.
- J. Yi, B. Zhang, P. Shao, Y. Li and W. Sun, *J. Phys. Chem. A*, 2010, **114**, 7055-7062.
- J. F. Zhang, C. S. Lim, B. R. Cho and J. S. Kim, *Talanta*, 2010, **83**, 658-662.
- D. Qiu, J. Wu, Z. Xie, Y. Cheng and L. Wang, *J. Organomet. Chem.*, 2009, **694**, 737-746.
- P.-H. Lanoe, J.-L. Fillaut, L. Toupet, J. A. G. Williams, H. Le Bozec and V. Guerschais, *Chem. Commun.*, 2008, 4333-4335.
- P.-H. Lanoë, H. Le Bozec, J. A. G. Williams, J.-L. Fillaut and V. Guerschais, *Dalton Trans.*, 2010, **39**, 707 - 710.
- P.-H. Lanoë, J.-L. Fillaut, V. Guerschais, H. Le Bozec and J. A. G. Williams, *Eur. J. Inorg. Chem.*, 2011, **8**, 1255-1259.
- C. Latouche, P.-H. Lanoe, J. A. G. Williams, V. Guerschais, A. Boucekkine and J.-L. Fillaut, *New J. Chem.*, 2011, **35**, 2196-2202.
- Q. Z. Yang, L. Z. Wu, H. Zhang, B. Chen, Z. X. Wu, L. P. Zhang and C. H. Tung, *Inorg. Chem.*, 2004, **43**, 5195-5197.
- J.-L. Fillaut, H. Akdas-Kilig, E. Dean, C. Latouche and A. Boucekkine, *Inorg. Chem.*, 2013, **52**, 4890-4897.
- W. R. Browne and B. L. Feringa, *Nature nanotech.*, 2006, **1**, 25-35.
- D. Bléger, Z. Yu and S. Hecht, *Chem. Commun.*, 2011, **47**, 12260-12266.
- Z. Mahimwalla, K. G. Yager, J.-i. Mamiya, A. Shishido, A. Priimagi and C. J. Barrett, *Polym. Bull.*, 2012, **69**, 967-1006.
- S. Venkataramani, U. Jana, M. Dommaschk, F. Sönnichsen, F. Tuczek and R. Herges, *Science*, 2011, **331**, 445-448.
- X. Zhang, Y. Wen, Y. Li, G. Li, S. Du, H. Guo, L. Yang, L. Jiang, H. Gao and Y. Song, *J. Phys. Chem. C*, 2008, **112**, 8288-8293.
- S. Tamesue, Y. Takashima, H. Yamaguchi, S. Shinkai and A. Harada, *Angew. Chem.*, 2010, **122**, 7623-7626.
- Y. Inoue, P. Kuad, Y. Okumura, Y. Takashima, H. Yamaguchi and A. Harada, *J. Am. Chem. Soc.*, 2007, **129**, 6396-6397.

20. F. Puntoriero, P. Ceroni, V. Balzani, G. Bergamini and F. Vögtle, *J. Am. Chem. Soc.*, 2007, **129**, 10714-10719.
21. J. Del Barrio, L. Oriol, R. Alcalá and C. Sánchez, *Macromolecules*, 2009, **42**, 5752-5760.
- 5 22. F. Ercole, T. P. Davis and R. A. Evans, *Polym. Chem.*, 2010, **1**, 37-54.
23. Y.-L. Zhao and J. F. Stoddart, *Langmuir*, 2009, **25**, 8442-8446.
24. D. Kim, S. Tripathy, L. Li and J. Kumar, *Appl. Phys. Lett.*, 1995, **66**, 1166-1168.
- 10 25. N. Viswanathan, D. Kim and S. Tripathy, *J. Mater. Chem.*, 1999, **9**, 1941-1955.
26. T. Fukuda, H. Matsuda, T. Shiraga, T. Kimura, M. Kato, N. K. Viswanathan, J. Kumar and S. K. Tripathy, *Macromolecules*, 2000, **33**, 4220-4225.
- 15 27. S. Hvilsted, C. Sánchez and R. Alcalá, *J. Mater. Chem.*, 2009, **19**, 6641-6648.
28. A. Shishido, *Polym. J.*, 2010, **42**, 525-533.
29. A. A. Beharry and G. A. Woolley, *Chem. Soc. Rev.*, 2011, **40**, 4422-4437.
- 20 30. J. Griffiths, *Chem. Soc. Rev.*, 1972, **1**, 481-493.
31. D. Gegiou, K. Muszkat and E. Fischer, *J. Am. Chem. Soc.*, 1968, **90**, 3907-3918.
32. D. R. Matazo, R. A. Ando, A. C. Borin and P. S. Santos, *J. Phys. Chem. A*, 2008, **112**, 4437-4443.
- 25 33. Y. Kuroda, H. Lee and A. Kuwae, *J. Phys. Chem.*, 1980, **84**, 3417-3423.
34. H. Y. Lee, A. s. Olsaz, C.-H. Chen and D. Lee, *Org. Lett.*, 2012, **14**, 6286-6289.
35. A. Dirksen, E. Zuidema, R. Williams, L. De Cola, C. Kauffmann, F. Vögtle, A. Roque and F. Pina, *Macromolecules*, 2002, **35**, 2743-2747.
36. S. Samanta, P. Ghosh and S. Goswami, *Dalton Trans.*, 2012, **41**, 2213-2226.
37. Y. Hasegawa, T. Nakagawa and T. Kawai, *Coord. Chem. Rev.*, 2010, **254**, 2643-2651.
38. Y. Hasegawa, S. Kume and H. Nishihara, *Dalton Trans.*, 2009, **2**, 280-284.
39. S. Thies, H. Sell, C. Schütt, C. Bornholdt, C. Näther, F. Tuczek and R. Herges, *J. Am. Chem. Soc.*, 2011, **133**, 16243-16250.
- 40 40. K. N. Gherab, R. Gatri, Z. Hank, B. Dick, R.-J. Kutta, R. Winter, J. Luc, B. Sahraoui and J.-L. Fillaut, *J. Mater. Chem.*, 2010, **20**, 2858-2864.
41. J. Kubitschke, C. Näther and R. Herges, *Eur. J. Org. Chem.*, 2010, **2010**, 5041-5055.
- 45 42. K. Suzuki, A. Kobayashi, S. Kaneko, K. Takehira, T. Yoshihara, H. Ishida, Y. Shiina, S. Oishi and S. Tobita, *Phys. Chem. Chem. Phys.*, 2009, **11**, 9850-9860.
43. A. Altomare, M. C. Burla, M. Camalli, G. L. Cascarano, C. Giacovazzo, A. Guagliardi, A. G. Moliterni, G. Polidori and R. Spagna, *J. Appl. Crystallogr.*, 1999, **32**, 115-119.
- 50 44. G. Sheldrick, *Acta Cryst A64*, 2008, 112-122.
45. L. J. Farrugia, *J. Appl. Crystallogr.*, 1999, **32**, 837-838.
46. C. Lee, W. Yang and R. G. Parr, *Phys. Rev. B*, 1988, **37**, 785-789.
47. A. D. Becke, *J. Chem. Phys.*, 1993, **98**, 5648-5652.
- 55 48. P. J. Stephens, F. J. Devlin, C. F. Chabalowski and M. J. Frisch, *J. Chem. Phys.*, 1994, **98**, 11623-11627.
49. P. J. Hay and W. R. Wadt, *J. Chem. Phys.*, 1985, **82**, 299-310.
50. M. J. Frisch, G. W. Trucks, H. B. Schlegel, G. E. Scuseria, M. A. Robb, J. Cheeseman, G. Scalmani, V. Barone, B. Mennucci, G. A. Petersson, H. Nakatsuji, M. Caricato, X. Li, H. P. Hratchian, A. F. Izmaylov, J. Bloino, G. Zheng, J. L. Sonnenberg, M. Hada, M. Ehara, K. Toyota, R. Fukuda, J. Hasegawa, M. Ishida, T. Nakajima, Y. Honda, O. Kitao, H. Nakai, T. Vreven, J. A. J. Montgomery, J. E. Peralta, F. Ogliaro, M. Bearpark, J. J. Heyd, E. Brothers, K. N. Kudin, V. N. Staroverov, R. Kobayashi, J. Normand, K. Raghavachari, A. Rendell, J. C. Burant, S. S. Iyengar, J. Tomasi, M. Cossi, N. Rega, J. M. Millam, M. Klene, J. E. Knox, J. B. Cross, V. Bakken, C. Adamo, J. Jaramillo, R. Gomperts, R. E. Stratmann, O. Yazyev, A. J. Austin, R. Cammi, C. Pomelli, J. W. Ochterski, R. L. Martin, K. Morokuma, V. G. Zakrzewski, G. A. Voth, S. P., J. J. Dannenberg, S. Dapprich, A. D. Daniels, O. Farkas, J. B. Foresman, J. V. Ortiz, J. Cioslowski and D. J. Fox, in GAUSSIAN 09, revision A. 02; Gaussian, Inc., Wallingford CT, 2009.
51. M. Cossi, G. Scalmani, N. Rega and V. Barone, *J. Chem. Phys.*, 2002, **117**, 43-54.
52. V. Barone, M. Cossi and J. Tomasi, *J. Chem. Phys.*, 1997, **107**, 3210-3221.
- 50 53. U. Varetto, Swiss National Supercomputing Centre: Lugano.
54. S. I. Gorelsky, Swizard program, revision 4.5, <http://www-sg-chem.net/swizard>.
55. S. I. Gorelsky, AOMix: Program for Molecular Orbital Analysis, University of Ottawa, <http://www-sg-chem.net/>, 2009.
- 85 56. P. Shao, Y. Li and W. Sun, *J. Phys. Chem. A*, 2008, **112**, 1172-1179.
57. H. D. Bandara and S. C. Burdette, *Chem. Soc. Rev.*, 2012, **41**, 1809-1825.
58. M. L. Clark, S. Diring, P. Retailleau, D. R. McMillin and R. Ziessel, *Chem. Eur. J.*, 2008, **14**, 7168-7179.
- 90 59. P. Shao, Y. Li, J. Yi, T. M. Pritchett and W. Sun, *Inorg. Chem.*, 2010, **49**, 4507-4517.
60. J.-F. Halet and C. Lapinte, *Coord. Chem. Rev.*, 2013, **257**, 1584-1613.
61. X. Han, L.-Z. Wu, G. Si, J. Pan, Q.-Z. Yang, L.-P. Zhang and C.-H. Tung, *Chem. Eur. J.*, 2007, **13**, 1231-1239.
- 95 62. K. M.-C. Wong, W.-S. Tang, X.-X. Lu, N. Zhu and V. W.-W. Yam, *Inorg. Chem.*, 2005, **44** 1492-1498.